Analytical and Bioanalytical Chemistry (2022) 414:3593–3603
https://doi.org/10.1007/s00216-022-03986-9

RESEARCH PAPER

A sensitive cholesterol electrochemical biosensor based on biomimetic cerasome and graphene quantum dots

Shuyao Wu[1] · Meijiao Jiang[1] · Hui Mao[1] · Nan Zhao[1] · Dongqing He[1] · Qinan Chen[1] · Daliang Liu[1] · Wei Zhang[1] · Xi-Ming Song[1]

Received: 8 January 2022 / Revised: 14 February 2022 / Accepted: 22 February 2022 / Published online: 26 February 2022

Abstract

A simple and sensitive electrochemical cholesterol biosensor was fabricated based on ceramic-coated liposome (cerasome) and graphene quantum dots (GQDs) with good conductivity. The cerasome consists of a lipid-bilayer membrane and a ceramic surface as a soft biomimetic interface, and the mild layer-by-layer self-assembled method as the immobilization strategy on the surface of the modified electrode was used, which can provide good biocompatibility to maintain the biological activity of cholesterol oxidase (ChOx). The GQDs promoted electron transport between the enzyme and the electrode more effectively. The structure of the cerasome-forming lipid was characterized by Fourier transform infrared (FT-IR). The morphology and characteristics of the cerasome and GQDs were characterized by transmission electron microscopy (TEM), zeta potential, photoluminescence spectra (PL), etc. The proposed biosensors revealed excellent catalytic performance to cholesterol with a linear concentration range of 16.0×10^{-6}–6.186×10^{-3} mol/L, with a low detection limit (LOD) of 5.0×10^{-6} mol/L. The Michaelis–Menten constant (K_m) of ChOx was 5.46 mmol/L, indicating that the immobilized ChOx on the PEI/GQDs/PEI/cerasome–modified electrode has a good affinity to cholesterol. Moreover, the as-fabricated electrochemical biosensor exhibited good stability, anti-interference ability, and practical application for cholesterol detection.

Keywords Cerasome · Graphene quantum dots · Cholesterol oxidase · Cholesterol · Electrochemical biosensor

Introduction

Cholesterol is widely found in the human body, especially in brain and nerve tissues. It is present in high amounts in the kidneys, spleen, skin, liver, and bile, and is necessary for life activities [1]. If the concentration of cholesterol exceeds the normal level in the body, it will cause cardiovascular disease, etc. [2]. When the cholesterol concentration is too low, it often leads to a decrease in the synthesis of corticosteroids, which results in weakened stress ability, immunity, and normal disease resistance [3]. Therefore, the detection of cholesterol level in serum is of great significance [4]. Several methods have been developed for the detection of cholesterol in blood, including colorimetry [5], spectrophotometry [6], chemiluminescence [7], and electrochemical methods [8, 9]. Among these methods, the electrochemical method based on cholesterol oxidase (ChOx) has been widely used due to its advantages of higher sensitivity and selectivity, lower price, and ease of operation [10, 11]. In addition, the electrode materials are particularly important for the construction of a cholesterol electrochemical biosensor. Therefore, the selectivity of electrode materials can availably improve the performance of electrochemical biosensors with a higher sensitivity and lower detection limit.

Liposomes, a biomimetic material with a cell-like membrane structure, have excellent compatibility with biomolecules. Using the membrane-like properties of liposomes as supporting matrix to modify the electrode surface is more beneficial to the binding of redox active biomolecules to the electrode [12]. However, it is difficult for liposomes to maintain the stability of their morphology on the solid surface, and they are often flattened into lipid bilayers, which greatly enhance the resistivity in the construction of electrochemical biosensors. Ceramic-coated liposome (cerasome) is an organic–inorganic hybrid material [13]. Its internal lipid bilayer and surface silicate

✉ Xi-Ming Song
songlab@lnu.edu.cn

[1] Liaoning Key Laboratory for Green Synthesis and Preparative Chemistry of Advanced Materials, College of Chemistry, Liaoning University, Shenyang 110036, China

network structure determine that the cerasome not only has good biocompatibility, but also can maintain its stable morphological structure on the electrode [12, 14]. Based on these advantages, it has been reported that the cerasome was used as a preferable electrode material to construct modified electrodes through non-covalent interaction with hydrophobic vitamin B_{12} derivatives or with hemoglobin [15, 16]. The results showed that cerasome had good electrochemical performance for the modification of the electrode. Furthermore, the double-lipid membrane structure of the cerasome can have a concentrated effect toward a water-insoluble substrate, like cholesterol [17]. Although SiO_2 nanoparticles with similar structure can also be used as supporting materials for biologically active enzymes, their poor biocompatibility is likely to lead to the inactivation of biomolecules, and poor conductivity is not suitable as an electrode material. It is expected that high-performance electrochemical biosensors can be prepared [18]. In order to increase the load of bioactive molecules and increase the electron transport capacity between the enzyme and electrode, the modified electrode was preferably constructed using the materials with large specific surface area and electrical conductivity.

As a zero-dimensional carbon nanomaterial, graphene quantum dots (GQDs) possess the characteristics of both graphene and quantum dots [19]. Due to their many excellent physical and chemical properties, such as excellent electrical conductivity, large surface area, good dispersibility, hypotoxicity, etc. [20–22], GQDs have attracted great attention for their application prospect in the field of electrochemical sensing [23, 24]. Razmi et al. [25] used GQDs as a substrate to successfully immobilize glucose oxidase (GOx) on a carbon ceramic electrode. The glucose biosensor presented a wide detection range, high sensitivity, high enzyme capacity, and good affinity for glucose, all of which are attributed to the advantages of GQDs with a large specific surface area and excellent electrical conductivity [26].

In this work, the novel biomimetic nanomaterial cerasomes with good biocompatibility and structural stability were prepared by ethanol injection method, and GQDs were simply prepared by acid oxidation of carbon black. The cerasome and the GQDs were used to construct ChOx/PEI/GQDs/PEI/cerasome–modified electrodes for the detection of cholesterol. The catalytic activity of the immobilized ChOx was well maintained, and the lipid-bilayer membrane structure of cerasome provided a good affinity for the substrate cholesterol, making the ChOx preferably interact with cholesterol. Moreover, the GQDs used in the construction of cerasome-based modified electrodes more effectively promoted electron transport between the enzyme and the electrode. The as-fabricated biosensor showed good performance in the detection of cholesterol.

Experimental

Reagents

Silicone (C-300 Silica Gel C-300), hydrochloric acid (HCl), nitric acid (HNO_3), anhydrous dichloromethane (CH_2Cl_2), ethyl acetate ($C_4H_8O_2$), anhydrous ethanol (C_2H_5OH), and cholesterol were purchased from Sinopharm Chemical Reagent Co., Ltd. Carbon black and polyethyleneimine (PEI) were obtained from Aladdin Reagent Co., Ltd. Cholesterol oxidase (ChOx, E.C.1.1.3.6, 500 U) was purchased from Sigma-Aldrich Chemical Co., Ltd. Hexadecylamine, hexadecyl bromide, potassium carbonate (K_2CO_3), ascorbic acid (AA), glucose (Glc), uric acid (UA), lactic acid (LA), and 3-(triethoxysilyl) propyl isocyanate were obtained from Alfa Aesar. Chloroform, methanol, N-hexane, and isopropanol were purchased from Tianjin Bodi Chemical Co., Ltd. All chemicals and reagents were of analytical grade and used without further purification. 0.1 mol/L phosphate buffer solutions (PBS, pH 7.0) were employed as supporting electrolyte. All solutions were prepared using ultrapure water (> 18.0 MΩ·cm).

Apparatus

The morphology of GQDs was observed using a model JEM-2100 transmission electron microscope (TEM) (Hitachi Corp., Japan). The Fourier transform infrared (FT-IR) spectra of the samples were measured utilizing a Spectrum One spectrophotometer (Perkin Elmer Corp., USA). Nuclear magnetic resonance (^{1}H NMR) was performed by a Mercury300 nuclear magnetic resonance spectrometer (Varian Corp., USA). Ultraviolet–visible spectroscopy (UV–vis) spectra were collected using a Lambda 35 spectrophotometer (Perkin Elmer Corp., USA). Zeta potential data were obtained using a Zetasizer Nano-ZS particle analyzer (Malvern Corp., England). Photoluminescence (PL) spectra were performed by a RF-5301PC fluorescence spectrophotometer (Shimadzu Corp., Japan). Cyclic voltammogram (CV) and differential pulse voltammogram (DPV) measurements were obtained using a CHI660E electrochemical workstation (Shanghai Chenhua Instruments Co., China). A conventional three-electrode system contained a platinum wire as auxiliary electrode, an Ag/AgCl electrode as reference electrode, and an as-prepared modified glassy carbon electrode (GCE, 3 mm, Shanghai Chenhua Instruments Co., China) as working electrode. All the electrochemical measurements were carried out in nitrogen environment at room temperature without particular illustration.

Preparation of N,N-dihexadecylamine $HN(C_{16}H_{33})_2$

10.0 g (41.4 mmol) hexadecylamine was dissolved in 40 mL of ethanol, and 6.0 g (19.7 mmol) hexadecyl bromide was added into it. Then, 9 g (65.1 mmol) K_2CO_3 was added and refluxed at 85 ℃ for 165 h. Afterwards, the solvent ethanol was removed by rotary evaporation, and the crude product was washed with deionized water 3 times to remove potassium carbonate. Finally, the crude product was dried in a vacuum oven.

The crude product was recrystallized with N-hexane 3 times, and the mixture of chloroform and methanol (9:1 v/v) was used as the developing solvent. The purity of the product after recrystallization was determined by thin-layer chromatography (TLC) (R_f = 0.43). The purified product was vacuum dried to a white flake solid with a yield of 44.5% [27].

Preparation of cerasome-forming lipids $(EtO)_3SiC_3U2C_{16}$

0.499 g (1.07 mmol) N,N-dihexadecylamine was placed in a round-bottom flask, and 30 mL anhydrous CH_2Cl_2 was added to completely dissolve the hexadecanamine. 0.320 g (1.29 mmol) 3-(triethoxyl) propyl isocyanate under nitrogen protection was added to the round-bottom flask and reacted for 2 h at room temperature. After the reaction, the solvent CH_2Cl_2 was removed by rotary evaporation to obtain a colorless viscous liquid. The crude product was purified by 300 mesh silica gel column chromatography with the eluent of n-hexane: ethyl acetate (4:1 v/v). The solvent was removed by rotary evaporation, and a colorless transparent viscous liquid was obtained after being dried with a rotary vacuum evaporator. The reaction yield was 62.3%. The product was sealed and dried in a refrigerator.

Preparation of cerasome

3.9 mg (5.45 mol) $(EtO)_3SiC_3U2C_{16}$ was placed in an oscillating tube. 1.9 μL (10 mmol/L) HCl solution and 63.5 μL (1.09 mmol) anhydrous ethanol were added to the mixture to vibrate for 12 h. A 0.5 mmol/L cerasome suspension was obtained by injecting 30 μL of the hydrolysate into 5 mL 40 ℃ deionized water at a slow and uniform rate under stirring conditions, then incubated at room temperature for 24 h [27].

Preparation of graphene quantum dots

0.25 g XC-72 carbon black was placed in a 100-mL round-bottom flask; 50 mL 6 mol/L HNO_3 was added and refluxed at 95 ℃ for 24 h under stirring. The resulting suspension was cooled to room temperature, centrifuged at 6000 RPM for 30 min to obtain a yellow supernatant, and then dried at 75 ℃. Finally, the red–brown graphene quantum dots (GQDs) were obtained [28].

Preparation of ChOx/PEI/GQDs/PEI/cerasome/GCE

A 7-μL cerasome (0.5 mmol/L) dispersion in water was dropped on the surface of the electrode. Water was slowly evaporated, and a layer of cerasome film was formed on the electrode surface at room temperature. Then, the electrode was immersed in 1 mg/mL PEI solution for 5 min at room temperature, rinsed with ultrapure water, and dried with nitrogen gas. After that, the PEI/cerasome/GCE was immersed in the aqueous dispersion of GQDs for 5 min; then, the above steps were repeated, with the electrode soaked in PEI. Finally, the electrode was immersed in 0.5 mg/mL ChOx (pH 8.0 PBS) solution under 4 ℃ for 24 h to obtain the ChOx/PEI/GQDs/PEI/cerasome/GCE.

Electrochemical measurements

The performances of the modified electrodes were investigated by a three-electrode system using an Ag/AgCl reference electrode and a platinum counter electrode. The GCE electrode modified with ChOx/PEI/GQDs/PEI/cerasome as the working electrode was rinsed with ultrapure water prior to use to remove the unadsorbed ChOx. Before the electrochemical experiment, high-purity nitrogen was inleted to 10 mL PBS for 30 min to remove oxygen. Electrochemical catalytical experiments were carried out under saturated oxygen condition.

The electrochemical impedance was tested with a frequency range of 0.1 Hz to 100 kHz, an AC voltage of 5 mV, and a solution containing 0.1 mol/L KCl with a concentration of 5.0 mmol/L $K_3[Fe(CN)_6]/K_4[Fe(CN)_6]$ (1:1).

Results and discussion

Characterization of N,N-dihexadecylamine $HN(C_{16}H_{33})_2$ and cerasome

Figure S1 shows the FT-IR spectra of $HN(C_{16}H_{33})_2$ (a) and cerasome (b). The absorption peaks of bending vibration and stretching vibration for C–H were 1467 cm^{-1} and 2920 cm^{-1}, respectively. The methyl absorption peak was at 1375 cm^{-1}, the characteristic peak at 1129 cm^{-1} was attributed to the C–N stretching vibration, and the characteristic methylene absorption peak was at 773 cm^{-1} and 726 cm^{-1} [12]. As for the cerasome, the intense bands at 1095 cm^{-1} and 953 cm^{-1} were corresponding to the stretching vibration peak of Si–O–Si and the stretching vibration peak of Si–OH bond, respectively. While the band at 783 cm^{-1} could be ascribed to the in-plane

bending vibration peak of the C–H bond. The bands around 1628 cm^{-1} and 1540 cm^{-1} could be assigned to the absorption peaks of the amide bond, indicating that the siloxane structure existed on the surface of cerasome, similar to SiO_2 nanoparticles [29].

Figure 1 is the TEM image of cerasome (a), the photo of the cerasome suspension under natural light (b), and the zeta potential diagram (c). It could be seen that the prepared cerasome was spherical-like, with a size between 200 and 300 nm (Fig. 1a), and the aqueous solution was milky white, which could maintain a stable state for a long time (Fig. 1b). The surface charge of the as-prepared cerasome was negative, and the zeta potential was – 44.7 mV, which was caused by Si–OH on the cerasome surface and the amide bond structure in the liposome monomer (Fig. 1c). This negative charge allowed the cerasome to disperse stably in aqueous solution for a long time without aggregation and precipitation, and provided a premise for further assembly of modified electrodes through electrostatic interaction. In addition, the surface of the cerasome was covered with rigid inorganic layers and the existence of intermolecular hydrogen bonds greatly improved the stability of the cerasome.

Morphology and structure characterization of graphene quantum dots

The morphology properties of GQDs were characterized as shown in Fig. 2a. The GQDs with a relatively uniform particle size and an average particle size of about 6 nm could be observed in the TEM image. Figure 2b, c shows the comparison photographs of the GQD aqueous dispersion under sunlight and ultraviolet light. It could be seen from Fig. 2b that the GQDs could form a uniform and stable red–brown dispersion with certain turbidity in water, and the dispersion of GQDs could remain stable for a long time at room temperature. Figure 2c shows the image of the GQD aqueous dispersion irradiated by an ultraviolet lamp. Under ultraviolet irradiation of 365 nm wavelength, the GQD aqueous dispersion emitted green fluorescence, while this phenomenon did not appear under sunlight, indicating that the GQDs were successfully prepared and had typical quantum dot properties [30].

Figure 2d is the zeta potential diagram of the GQD aqueous dispersion. The zeta potential test results showed that the GQDs presented a relatively strong negative charge, and zeta potential value was – 19.3 mV. The strong electrostatic repulsion between surface charges could effectively prevent the aggregation of GQD molecules, so that the GQDs could

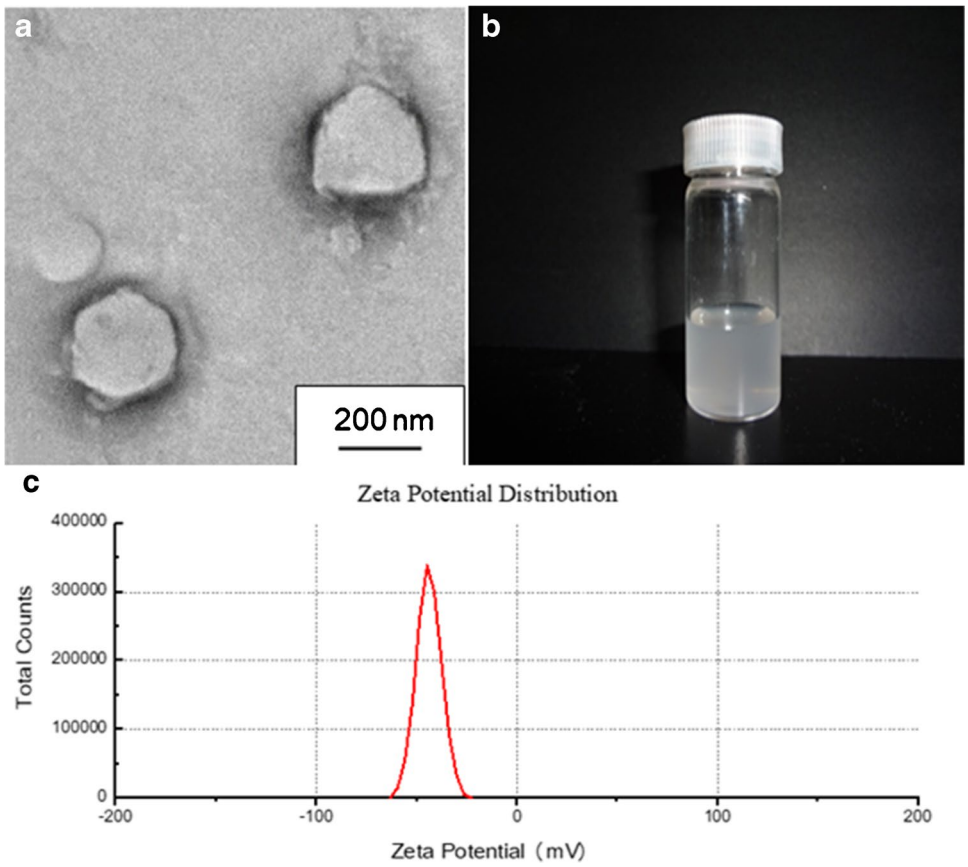

Fig. 1 **a** TEM image of cerasome; **b** photographs of cerasome solution under normal light; **c** zeta potential data of cerasome in the aqueous dispersion

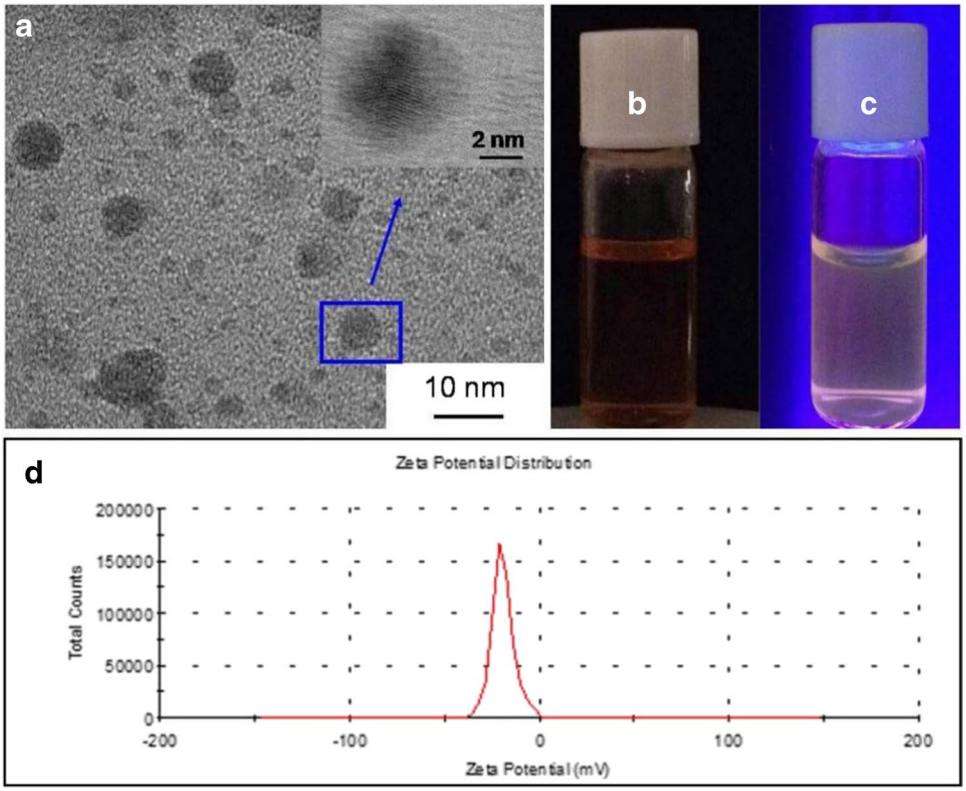

Fig. 2 **a** TEM image of as-prepared GQDs; **b** photographs of GQD solution under normal light and **c** monochromatic light of 365 nm; **d** zeta potential data of GQDs in the aqueous dispersion

be stably stored in water for a long time. In addition, the negative charge on the surface of the GQDs provided preconditions for further preparation of enzyme-modified electrodes by electrostatic adsorption.

Figure 3a is the FT-IR spectrum of the GQDs. The bands around 1373 cm^{-1} could be assigned to –COOH stretching vibration. The intense bands at 1713 cm^{-1} and 3518 cm^{-1}, correspond to the C = O stretching and –OH hydroxyl association, while the band at 1049 cm^{-1} could be ascribed to the C–O stretching [31]. It could be seen from the spectrum of GQDs that a large number of carboxyl groups and hydroxyl functional groups existed in the GQDs.

Figure 3b shows the UV–vis and PL spectra of the GQD aqueous dispersion. It could be seen that a broad absorption peak appeared at a wavelength of 301 nm; it was related to the n-π* transitions of aromatic C = O bonds [32]. As the excitation wavelength increased, the fluorescence intensity decreased, and the peak position shifted to the right. The best excitation wavelength was 300 nm. It shows the fluorescence characteristic of quantum dots and proved the successful preparation of GODs.

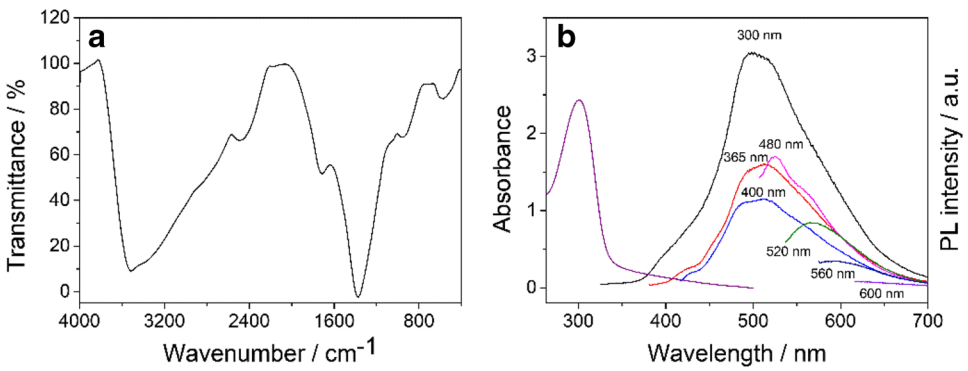

Fig. 3 **a** FT-IR spectrum of GQDs; **b** UV–vis absorption and PL emission spectra of GQD aqueous dispersion

Electrochemical performance studies of ChOx/PEI/GQDs/PEI/cerasome/GCE

Construction of ChOx/PEI/GQDs/PEI/cerasome/GCE

The construction process of ChOx/PEI/GQDs/PEI/cerasome/GCE is shown in Fig. 4. First, the cerasome was dropped on the electrode surface which could adsorb positively charged PEI, and then interacted with negatively charged GQDs and adsorb PEI again. Since ChOx is an amphoteric protein, ChOx has a negative charge when the pH is higher than its isoelectric point. When PEI/GQDs/PEI/cerasome/GCE was immersed in the negatively charged ChOx suspension, the enzyme molecules could be adsorbed to the surface of PEI/GQDs/PEI/cerasome through electrostatic interaction to obtain ChOx/PEI/GQDs/PEI/cerasome/GCE. The advantage of using electrostatic interaction for molecular self-assembly is that it enables enzymes to be immobilized on the surface of nanomaterials under relatively mild conditions, so that the natural structure and bioelectrical activity of the immobilized enzymes can be effectively maintained [33].

The influence of pH on ChOx/PEI/GQDs/PEI/cerasome/GCE

Since protons participated in the entire electrode reaction, the redox peak of ChOx should be affected by the pH change of the solution [4]. The performance of ChOx/PEI/GQDs/PEI/cerasome/GCE was investigated by cyclic voltammograms (CVs) at pH 4.0–8.0 in PBS. It is evident from Fig. S2A that both oxidation peak and reduction peak move toward the negative potential with the increase of pH, indicating that the electrochemical behavior of ChOx was affected by pH. As shown in Fig. S2B, the linear relationship between the equation potential and pH, and the slope is − 50.3 mV/pH ($R = 0.999$), suggesting that the electron transport process of ChOx is a process of isoproton coupling [34].

The electrochemical properties of the ChOx/PEI/GQDs/PEI/cerasome/GCE

Figure 5A shows the CV curves of cerasome/GCE (a)– and PEI/GQDs/PEI/cerasome/GC (b)–modified electrodes at 0.1 mol/L PBS (pH 7.0). As shown, no redox peaks were observed in the figure, suggesting that both of the modified electrodes had no electrical activity within the scanning range. However, the ChOx/PEI/cerasome/GCE (a) and ChOx/PEI/GQDs/PEI/cerasome/GCE (b) electrodes had a pair of obvious redox peaks (Fig. 5B), and the GQD–modified electrode peak was larger, indicating that the electrode has better electron transport performance. The oxidation peak potential (E_{pa}) and the reduction peak potential (E_{pc}) were − 0.396 V and − 0.4441 V, respectively, with a peak potential separation of 45 mV. The formal potential (E_p), the average of E_{pc} and E_{pa}, was − 0.419 V. The redox peak current had good symmetry, indicating that the electrode reaction was a rapid electron transfer process and had good reversibility.

The CVs of the ChOx/PEI/GQDs/PEI/cerasome/GCE at various scan rates were investigated to evaluate the electron transfer kinetics. Figure 5C shows the CV curves at various scan rates ranging from 0.1 to 0.8 V/s, and the oxidation peak and the reduction peak current increased simultaneously, and had a good linear relationship with the scan rate (inset of Fig. 5C), suggesting that the electrode reaction process is a surface control process [18].

Electrochemical impedance spectroscopy was used to monitor the electrode layer-by-layer self-assembly process. In a typical Nyquist plot (Fig. 5D), the value of the electron transfer resistance at the electrode surface can be estimated from the diameters of the high-frequency semicircle. The linear part of the plot at lower frequency range is attributed to a diffusion-limited process. The impedance of cerasome/GCE showed a larger resistance value (curve a). After the PEI coated the modified electrode, the resistance value increased slightly (curve b). But when the GQDs assembled onto the electrode surface, the resistance value decreased

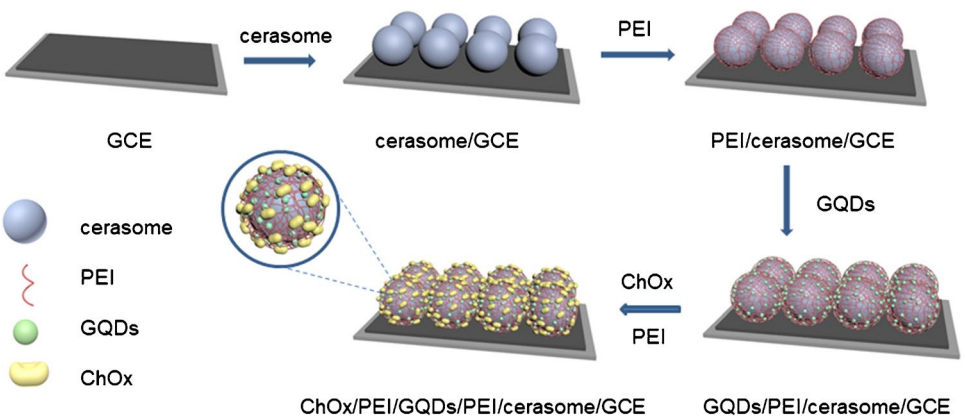

Fig. 4 Fabrication of ChOx/PEI/GQDs/PEI/cerasome/GCE

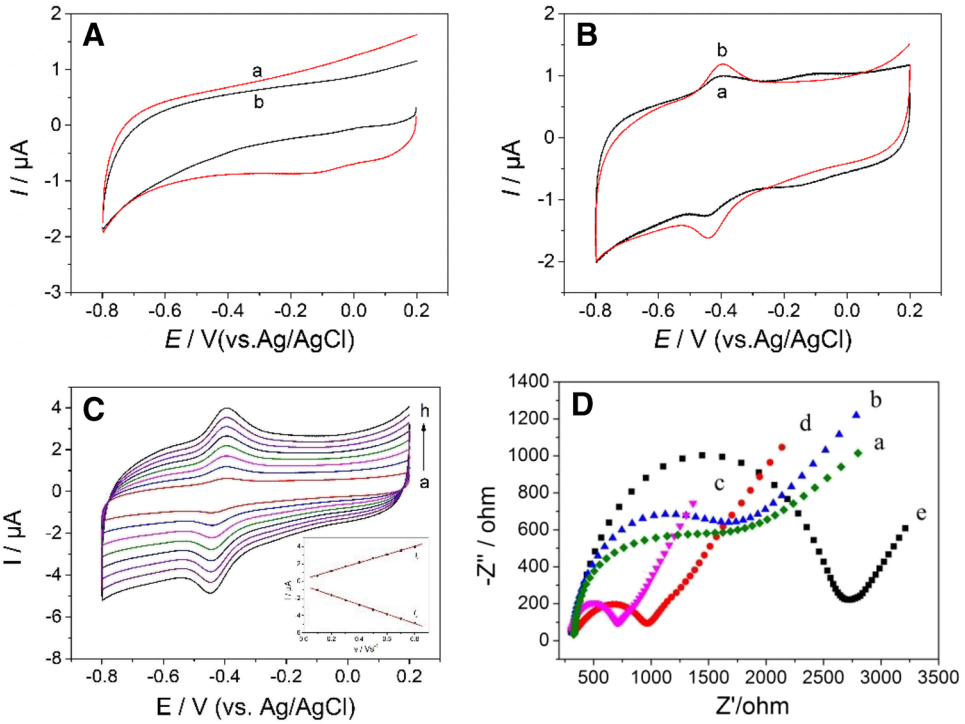

Fig. 5 **A** CVs of cerasome/GCE (a) and PEI/GQDs/PEI/cerasome/GCE (b); **B** ChOx/PEI/cerasome/GCE (a) and ChOx/PEI/GQDs/PEI/cerasome/GCE (b) in 0.1 mol/L PBS at pH 7.0; **B** CVs of ChOx/cerasome/GCE at scan rates of 0.1, 0.2, 0.3, 0.4, 0.5, 0.6, 0.7, and 0.8 V/s (a–h) in 0.1 mol/L PBS at pH 7.0 (inset: plots of oxidation peak current I_a and reduction peak current I_c versus scan rate); **D** Nyquist plots of cerasome/GCE (a), PEI/cerasome/GCE (b), GQDs/PEI/cerasome/GCE (c), PEI/GQDs/PEI/cerasome/GCE (d), and ChOx/PEI/GQDs/PEI/cerasome/GCE (e)

obviously (curve c), illustrating that the GQDs enhanced the conductivity of the modified electrode. After continuing to modify with the PEI, again, the resistance value is still slightly increased (curve d). Lastly, with the modification of the enzyme, the resistance value of the modified electrode increased significantly, indicating that ChOx was successfully immobilized on the modified electrode (curve e).

Study of the catalytic performance of ChOx/PEI/GQDs/PEI/cerasome/GCE for cholesterol

The rapid and sensitive detection of cholesterol is of great significance in clinical diagnosis [35]. In order to investigate the biocatalytic activity of ChOx on the modified electrodes, this experiment explored the catalytic response of ChOx/PEI/GQDs/PEI/cerasome/GCE to cholesterol. The three curves in Fig. 6A represent the CV curves in N_2-saturated PBS (a), 5.686 mmol/L cholesterol (b), and O_2-saturated (c), respectively. Obviously, the reduction peak current increased significantly after O_2 was introduced into the buffer solution comparing curve a, suggesting that the reducing state ($FADH_2$) of the ChOx coenzyme was oxidized to the oxidation state (FAD). After adding cholesterol, the reduction peak current decreased correspondingly (curve c), indicating that the ChOx had good catalytic performance for cholesterol.

Figure 6B shows the CV curves of ChOx/PEI/GQDs/PEI/cerasome/GCE in the presence of cholesterol in 0.1 mol/L PBS at pH 7.0. As the cholesterol concentration increased, the reduction peak current decreased, indicating that ChOx immobilized on PEI/GQDs/PEI/cerasome/GCE maintained a good catalytic activity for the reduction of cholesterol. It could be seen from Fig. 6C, D that the detection concentration range of the modified electrode for cholesterol was $16.0\times10^{-6}-6.186\times10^{-3}$ mol/L, the linear equation was $y=0.187x+0.037$, and the linear correlation coefficient R^2 was 0.999 (x was the concentration of cholesterol, y was the concentration of the cholesterol/response current value). The limit of detection (LOD) was calculated to be 5.0×10^{-6} mol/L according to the LOD $=3\sigma/S$ (where σ represents the standard deviation of peak currents of the blanks and S represents the slope of the calibration plot). The Michaelis constant (K_m) was estimated to be 5.46 mmol/L according to the Lineweaver–Burk equation: $1/i_{ss}=(K_m/i_{max})(1/C)+(1/i_{max})$, where i_{ss} is the current under steady state after the addition of cholesterol, i_{max} is the maximum current measured under saturated cholesterol conditions, and C is the cholesterol concentration. Compared to the other reported electrochemical biosensors for cholesterol determination, the as-fabricated electrochemical biosensors showed the lower LOD, wider linear range, and higher K_m value in our work (Table 1).

The repeatability, stability, and anti-interference performance of ChOx/PEI/GQDs/PEI/cerasome/GCE

To investigate the repeatability of the ChOx/PEI/GQDs/PEI/cerasome/GCE, five identical glassy carbon electrodes were

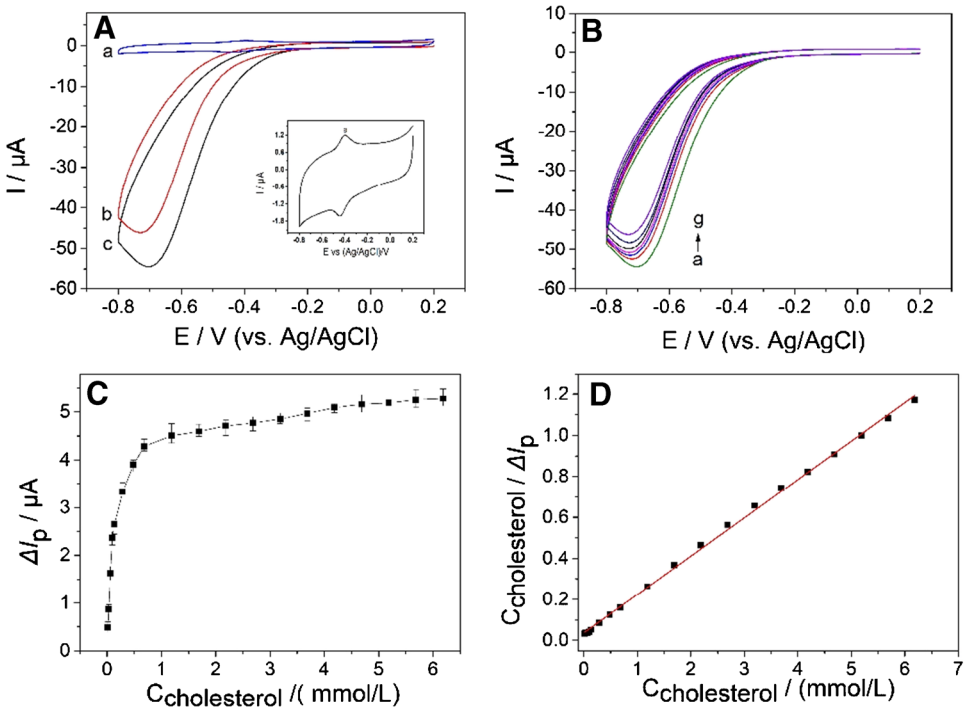

Fig. 6 **A** CVs of ChOx/PEI/GQDs/PEI/cerasome/GCE in N_2-saturated (a) and O_2-saturated 0.1 mol/L PBS with 5.686 mmol/L cholesterol (b) and in O_2-saturated at pH 7.0 PBS (c). Scan rate, 200 mV/s (Inset: amplification of curve a). **B** CVs of ChOx/PEI/GQDs/PEI/cerasome/GCE in O_2-saturated 0.1 mol/L PBS at pH 7.0 containing 0 (a), 0.096 (b), 0.286 (c), 1.186 (d), 3.186 (e), and 5.686 mmol/L (f) cholesterol. Scan rate, 200 mV/s. **C** Dependence of the electrocatalytic current change ΔI before and after addition of cholesterol on cholesterol concentration for ChOx/PEI/GQDs/PEI/cerasome/GCE. **D** Relationship between the cholesterol concentration/ΔI and cholesterol concentration

Table 1 Comparison of the reported cholesterol electrochemical biosensors

Electrode	Detection method	LOD μmol L^{-1}	Linear range μmol L^{-1}	R^2	K_m mmol L^{-1}	Reference
AgNPs/BDDE coupled with PAD[a]	Amperometry	6.5	10–7000	0.9967	6.48	[36]
ChOx-CSPPy-g-$C_3N_4H^+$/GCE[b]	Amperometry	8.0	20–5000	0.9988	52	[37]
PPy-NO^{3-}-$Fe(CN)_6^{4-}$-AuNPs-ChOx-CE[c]	Amperomety	25	5–25	0.98	–	[38]
AuNPs-f-MWCNT-PPy-ChOx/GCE[d]	Amperometry	100	2000–8000	0.9897	1.66	[3]
ChOx-gRGO-PPy/GCE[e]	DPV	3.78	10–6000	0.99	0.17	[39]
CoMnHCF/Nafion/ChOx[f]	CV	30	50–150	0.99	0.139	[40]
GCE/PTH/ChOx/HRP[g]	DPV	6.3	25–125	0.99	–	[41]
ChOx/Pt/rGO/P3ABA-modified SPCE[h]	Amperometry	40.5	250–4000	0.9927	3.82	[2]
Fe_3O_4@APTES-MNP[i]	CV	80	100–700	0.9882	–	[42]
Fe_3O_4@PAMAM-MNP[j]		100	100–800	0.9834	–	
ChOx/PEI/GQDs/PEI/cerasome/GCE	CV	5	16–6186	0.999	5.46	This work

[a]Silver nanoparticle/boron-doped diamond electrode coupled with paper-based analytical device

[b]ChOx/cylindrical spongy-shaped polypyrrole/graphitic carbon nitrides/GCE

[c]Pyrrole-NO^{3-}-$Fe(CN)_6^{4-}$-gold nanoparticles-cholesterol oxidase-cholesterol esterase

[d]ChOx immobilized on gold nanoparticles–functionalized–multiwalled carbon nanotube–polypyrrole nanocomposite modified electrode

[e]ChOx/green reduced graphene oxide/polypyrrole/GCE

[f]Hexacyanoferrate(III) containing Co^{2+} and Mn^{2+}/Nafion/ChOx

[g]GCE/poly(thionine)/ChOx/horseradish peroxidase

[h]ChOx/platinum/reduced graphene oxide/poly(3-aminobenzoic acid)/screen-printed carbon electrode

[i]Fe_3O_4 was functionalized with 3-aminopropyltriethoxysilane (APTES) magnetic nanoparticles

[j]Fe_3O_4 was functionalized with polyamidoamine (PAMAM) magnetic nanoparticles

used to prepare ChOx/PEI/GQDs/PEI/cerasome/GCE and the modified electrode was used to determine 0.5 mmol/L cholesterol; the test result showed that the relative standard deviation of the catalytic current was 3.4%, indicating that the modified electrode had good repeatability. Furthermore, the influence of storage time on the stability of ChOx/PEI/

GQDs/PEI/cerasome/GCE was also studied. The current response value did not change significantly after storing at 4 ℃ for a week (near 100% of its original value), suggesting its good stability.

In addition, the effect of adding interfering substances on the detection of cholesterol was investigated. The experimental results showed that there was no significant change in the electrochemical response signal of the sensor when 2 mmol/L AA, 2 mmol/L Glc, 0.2 mmol/L UA, and 0.2 mmol/L LA were added, suggesting that these interfering substances had no significant influence on the determination of cholesterol. These results further demonstrated the good selectivity and anti-interference ability of the as-fabricated biosensor.

Sample analysis

The potential applicability of the developed biosensor for cholesterol detection was studied by using human blood serum as real sample. The recovery of the biosensor was evaluated by the standard addition method. The DPV responses of the analyte samples (the appropriate concentration of the cholesterol standard solution) added into the real sample were recorded, respectively. The values of the recovery obtained were in the range of 96.0–105.0%. The obtained results (Table 2) revealed that the cholesterol detection of the as-fabricated biosensor in serum samples was acceptable and reliable.

Conclusions

In summary, the biomimetic cerasome with a phospholipid-bilayer structure was prepared with good biocompatibility and structural stability. The GQDs with good conductivity and cerasome were used to fabricate ChOx/PEI/GQDs/PEI/cerasome/GCE by assembling alternately the positively charged polyelectrolyte of PEI. A mild environment for enzyme immobilization was provided by the utilization of the layer-by-layer assembled method, which was conducive to keep the bioactivity of the redox enzyme. This bioelectrode exhibited good biosensing performance for cholesterol with a wide linear range, a low detection limit, and good selectivity and recoveries, benefiting by the lipid-bilayer membrane structure of cerasome, which was conducive to the long-term maintenance of enzyme biological activity and had a good affinity for cholesterol substrate, making ChOx more sensitive to catalysis oxidation of cholesterol. Moreover, the GQDs commendably promoted the electron transfer between ChOx and the electrode. This novel cholesterol biosensor might have a great prospect in clinical detection.

Table 2 Determination of the cholesterol in human serum by the proposed biosensor

Cholesterol spiked (mmol/L)	Cholesterol found[a] (mmol/L)	Recovery (%)
0.20	0.21 ± 0.07	105.0
0.50	0.48 ± 0.09	96.0
0.80	0.81 ± 0.12	101.3

[a]An average value from three determinations

Supplementary Information The online version contains supplementary material available at https://doi.org/10.1007/s00216-022-03986-9.

Acknowledgements The authors gratefully acknowledge the financial support from the National Natural Science Foundation of China (No. 51773085), the Liaoning University Doctor Start-up Fund (No. a280008020), the research fund pre-declaration project of Liaoning University (No. LDGY2019001), and the teaching reform research project of Liaoning University (No. JG2018YB20, LNDXJG20183013, JG2020ZSWT022).

Declarations

Conflict of interest The authors declare no competing interests.

References

1. Huang Y, Tan J, Cui L, Zhou Z, Zhao Y. Graphene and Au NPs co-mediated enzymatic silver deposition for the ultrasensitive electrochemical detection of cholesterol. Biosens Bioelectron. 2017;102:560–7. https://doi.org/10.1016/j.bios.2017.11.037.
2. Phetsang S, Jakmunee J, Mungkornasawakul P, Laocharoensuk R, Ounnunkad K. Sensitive amperometric biosensors for detection of glucose and cholesterol using a platinum/reduced graphene oxide/poly(3-aminobenzoic acid) film-modified screen-printed carbon electrode. Bioelectrochemistry. 2019;127:125–35. https://doi.org/10.1016/j.bioelechem.2019.01.008.
3. Alagappan M, Immanuel S, Sivasubramanian R, Kandaswamy A. Development of cholesterol biosensor using Au nanoparticles decorated f-MWCNT covered with polypyrrole network. Arab J Chem. 2020;13(1):2001–10. https://doi.org/10.1016/j.arabjc.2018.02.018.
4. Wu S, Hao J, Yang S, Sun Y, Wang Y, Zhang W, Mao H, Song X-M. Layer-by-layer self-assembly film of PEI-reduced graphene oxide composites and cholesterol oxidase for ultrasensitive cholesterol biosensing. Sens Actuators B: Chem. 2019;298:126856–64. https://doi.org/10.1016/j.snb.2019.126856.
5. Chung M, Jang YJ, Kim MI. Convenient colorimetric detection of cholesterol using multi-enzyme co-incorporated organic-inorganic hybrid nanoflowers. J Nanosci Nanotechnol. 2018;18(9):6555–61. https://doi.org/10.1166/jnn.2018.15697.
6. Islam JAH, Manuel SSL, Esther M, Guadalupe GL, Jesús LM. Cholesterol content in human milk during lactation: a comparative study of enzymatic and chromatographic methods. J Agric Food Chem. 2018;66(25):6373–81. https://doi.org/10.1021/acs.jafc.8b02205.
7. Javad H, Alireza K. Ultrasensitive chemiluminescent biosensor for the detection of cholesterol based on synergetic peroxidase-like activity of MoS_2 and graphene quantum dots. Talanta. 2018;178:992–1000.

8. Thakur N, Kumar M, Das Adhikary S, Mandal D, Nagaiah TC. PVIM–Co_5POM/MNC composite as a flexible electrode for the ultrasensitive and highly selective non-enzymatic electrochemical detection of cholesterol. Chem Commun. 2019;55(34):5021–4. https://doi.org/10.1039/c9cc01534e.
9. Abdi MM, Razalli RL, Tahir PM, Chaibakhsh N, Hassani M, Mir M. Optimized fabrication of newly cholesterol biosensor based on nanocellulose. Int J Biol Macromol. 2019;126:1213–22.
10. Rashidi K, Mahmoudi M, Mohammadi G, Zangeneh MM, Korani S, Goicoechea HC, Gu H-W, Jalalvand AR. Simultaneous co-immobilization of three enzymes onto a modified glassy carbon electrode to fabricate a high-performance amperometric biosensor for determination of total cholesterol. Int J Biol Macromol. 2018;120:587–95. https://doi.org/10.1016/j.ijbiomac.2018.08.163.
11. Huang Y, Cui L, Xue Y, Zhang S, Zhu N, Liang J, Li G. Ultrasensitive cholesterol biosensor based on enzymatic silver deposition on gold nanoparticles modified screen-printed carbon electrode. Mater Sci Eng, C. 2017;77:1–8. https://doi.org/10.1016/j.msec.2017.03.253.
12 Qiao Y, Tahara K, Zhang Q, Song XM, Kikuchi J. Cerasomes: soft interface for redox enzyme electrochemical signal transmission. Chemistry. 2016;22(4):1340–8. https://doi.org/10.1002/chem.201504042.
13. Kikuchi J, Yasuhara K. Cerasomes: a new family of artificial cell membranes with ceramic surface. INTECH Open Access Publisher. 2011;11:235–49.
14. Katagiri K, Ariga K, Kikuchi J. Preparation of organic-inorganic hybrid vesicle "cerasome" derived from artificial lipid with alkoxysilyl head. Chem Lett. 1999;7:661–2. https://doi.org/10.1246/cl.1999.661.
15. Liu D, Zhuang Q, Zhang L, Zhang H, Song XM. Self-assembly of novel fluorescent quantum dot-cerasome hybrid for bioelectrochemistry. Talanta. 2016;154:31–7.
16. Qiao Y, Tahara K, Zhang Q, Song X-M, Hisaeda Y, J-iJCL K. Construction of molecular communication interface formed from cerasome and hydrophobic vitamin B_{12} on glassy carbon electrode. Chem Lett. 2014;43(5):684–6. https://doi.org/10.1246/cl.140025.
17. Zhang Y, Li Q, Dong M, Han X. Effect of cholesterol on the fluidity of supported lipid bilayers. Colloids Surf B. 2020;196:111353. https://doi.org/10.1016/j.colsurfb.2020.111353.
18. Wu S, Chen J, Liu D, Zhuang Q, Pei Q, Xia L, Zhang Q, Kikuchi JI, Hisaeda Y, Song XMJRA. A biocompatible cerasome based platform for direct electrochemistry of cholesterol oxidase and cholesterol sensing. RSC Adv. 2016;6(75):70781–90.
19. Yan Y, Gong J, Chen J, Zeng Z, Huang W, Pu K, Liu J, Chen P. Recent advances on graphene quantum dots: fromchemistry and physics to applications. Adv Mater. 2019;31(21):1808283. https://doi.org/10.1002/adma.201808283.
20. Zhao J, Chen G, Zhu L, Li G. Graphene quantum dots-based platform for the fabrication of electrochemical biosensors. Electrochem Commun. 2011;13(1):31–3.
21. Shaker M, Riahifar R, Li YJF. A review on the superb contribution of carbon and graphene quantum dots to electrochemical capacitors performance: synthesis and application. Flatchem. 2020;22:100171.
22. Tan W, Renjun H, Kong Y, Yueguo Q. Preparation of nitrogen-doped carbon using graphene quantum dots-chitosan as the precursor and its supercapacitive behaviors. Int J Biol Macromol. 2018;112:561–6.
23. Huang J-Y, Zhao L, Lei W, Wen W, Wang Y-J, Bao T, Xiong H-Y, Zhang X-H, Wang S-F. A high-sensitivity electrochemical aptasensor of carcinoembryonic antigen based on graphene quantum dots-ionic liquid-nafion nanomatrix and DNAzyme-assisted signal amplification strategy. Biosens Bioelectron. 2018;99:28–33. https://doi.org/10.1016/j.bios.2017.07.036.
24. Bhardwaj H, Marquette CA, Dutta P, Rajesh SG. Integrated graphene quantum dot decorated functionalized nanosheet biosensor for mycotoxin detection. Anal Bioanal Chem. 2020;412(25):7029–41. https://doi.org/10.1007/s00216-020-02840-0.
25. Razmi H, Mohammad-Rezaei R. Graphene quantum dots as a new substrate for immobilization and direct electrochemistry of glucose oxidase: application to sensitive glucose determination. Biosens Bioelectron. 2013;41(6):498–504.
26. Chen Y-C, Chiang W-H, Kurniawan D, Yeh P-C, Otake K-i, Kung C-W. Impregnation of graphene quantum dots into a metal-organic framework to render increased electrical conductivity and activity for electrochemical sensing. ACS Appl Mater Interfaces. 2019;11(38):35319–26. https://doi.org/10.1021/acsami.9b11447.
27. Sasaki Y, Matsui K, Aoyama Y, Kikuchi J. Cerasome as an infusible and cell-friendly gene carrier: synthesis of cerasome-forming lipids and transfection using cerasome. Nat Protoc. 2006;1(3):1227–34. https://doi.org/10.1038/nprot.2006.182.
28. Shen J, Zhu Y, Yang X, Li C. Cheminform abstract: graphene quantum dots: emergent nanolights for bioimaging, sensors, catalysis and photovoltaic devices. Chem Commun. 2012;48(31):3686–99. https://doi.org/10.1002/chin.201229273.
29. Li S, Yin G, Pu X, Huang Z, Liao X, Chen X. A novel tumor-targeted thermosensitive liposomal cerasome used for thermally controlled drug release. Int J Pharm. 2019;570:118660. https://doi.org/10.1016/j.ijpharm.2019.118660.
30. Jian X, Liu X, Yang H-m, Guo M-m, Song X-l, Dai H-y, Liang Z-h. Graphene quantum dots modified glassy carbon electrode via electrostatic self-assembly strategy and its application. Electrochim Acta. 2016;190:455–62. https://doi.org/10.1016/j.electacta.2016.01.045.
31. Li L-L, Ji J, Fei R, Wang C-Z, Lu Q, Zhang J-R, Jiang L-P, Zhu J-J. A facile microwave avenue to electrochemiluminescent two-color graphene quantum dots. Adv Funct Mater. 2012;22(14):2971–9. https://doi.org/10.1002/adfm.201200166.
32. Yan Y, Chen J, Li N, Tian J, Li K, Jiang J, Liu J, Tian Q, Chen P. Systematic bandgap engineering of graphene quantum dots and applications for photocatalytic water splitting and CO_2 reduction. ACS Nano. 2018;12(4):3523–32.
33. Zhang Y, Arugula MA, Wales M, Wild J, Simonian AL. A novel layer-by-layer assembled multi-enzyme/CNT biosensor for discriminative detection between organophosphorus and non-organophosphrus pesticides. Biosens Bioelectron. 2015;67:287–95. https://doi.org/10.1016/j.bios.2014.08.036.
34. Li X-R, Xu J-J, Chen H-Y. Potassium-doped carbon nanotubes toward the direct electrochemistry of cholesterol oxidase and its application in highly sensitive cholesterol biosensor. Electrochim Acta. 2011;56(25):9378–85. https://doi.org/10.1016/j.electacta.2011.08.020.
35. Wu S, Wang Y, Mao H, Wang C, Xia L, Zhang Y, Ge H, Song XMJRA. Direct electrochemistry of cholesterol oxidase and biosensing of cholesterol based on PSS/polymeric ionic liquid–graphene nanocomposite. RSC Adv. 2016;6:59487–96. https://doi.org/10.1039/C6RA06073K.
36. Nantaphol S, Chailapakul O, Siangproh W. A novel paper-based device coupled with a silver nanoparticle-modified boron-doped diamond electrode for cholesterol detection. Anal Chim Acta. 2015;891:136–43. https://doi.org/10.1016/j.aca.2015.08.007.
37. Shrestha BK, Ahmad R, Shrestha S, Park CH, Kim CS. In situ synthesis of cylindrical spongy polypyrrole doped protonated graphitic carbon nitride for cholesterol sensing application. Biosens Bioelectron. 2017;94:686–93. https://doi.org/10.1016/j.bios.2017.03.072.
38. Rahim MZA, Govender-Hondros G, Adeloju SB. A single step electrochemical integration of gold nanoparticles, cholesterol oxidase, cholesterol esterase and mediator with polypyrrole films for

fabrication of free and total cholesterol nanobiosensors. Talanta. 2018;189:418–28. https://doi.org/10.1016/j.talanta.2018.06.041.
39. Pramanik K, Sarkar P, Bhattacharyay D, Majumdar P. One step electrode fabrication for direct electron transfer cholesterol biosensor based on composite of polypyrrole, green reduced graphene oxide and cholesterol oxidase. Electroanalysis. 2018;30(11):2719–30. https://doi.org/10.1002/elan.201800318.
40. Antuch M, Matos-Peralta Y, Llanes D, Echevarria F, Rodriguez-Hernandez J, Marin MH, Diaz-Garcia AM, Reguera L. Bimetallic Co^{2+} and Mn^{2+} hexacyanoferrate for hydrogen peroxide electrooxidation and its application in a highly sensitive cholesterol biosensor. ChemElectroChem. 2019;6(5):1567–73. https://doi.org/10.1002/celc.201900190.
41. Rahman MM, Li XB, Kim J, Lim BO, Ahammad AJS, Lee JJ. A cholesterol biosensor based on a bi-enzyme immobilized on conducting poly(thionine) film. Sens Actuators B: Chem. 2014;202:536–42. https://doi.org/10.1016/j.snb.2014.05.114.
42. Doaga R, McCormac T, Dempsey E. Functionalized magnetic nanomaterials for electrochemical biosensing of cholesterol and cholesteryl palmitate. Microchim Acta. 2020;187(4):225. https://doi.org/10.1007/s00604-020-4203-1.